Original Article

Architectural Correlates of Myocardial Conduction AQ1

Changes to the Topography of Cellular Coupling, Intracellular Conductance, and Action Potential Propagation with Hypertrophy in Guinea-Pig Ventricular Myocardium

Christopher H. Fry, DSc; Rosaire P. Gray, MRCP, PhD Paramdeep S. Dhillon, MRCP, PhD; Rita I. Jabr, PhD; Emmanuel Dupont, PhD; Pravina M. Patel, BSc; Nicholas S. Peters, FRCP, MD; AQ3

Background—We tested the hypothesis that alterations to action potential conduction velocity (CV) and conduction anisotropy in left ventricular hypertrophy are associated with topographical changes to gap-junction coupling and intracellular conductance by measuring these variables in the same preparations. AQ5

Methods and Results—Left ventricular papillary muscles were excised from aortic-banded or sham-operated guinea-pig hearts. With intracellular stimulating and recording microelectrodes, CV was measured in 3 dimensions with simultaneous conductance mapping with subthreshold stimuli and correlated with quantitative histomorphometry of myocardial architecture and connexin 43 distribution. In hypertrophied myocardium, CV in the longitudinal axis was smaller and transverse velocity was greater compared with control; associated with similar differences of intracellular conductance, consistent with more cell contacts per cell (5.7±0.2 versus 8.1±0.5; control versus hypertrophy), and more intercalated disks mediating side-to-side coupling (8.2±0.2 versus 10.2±0.4 per cell). Intercalated disk morphology and connexin 43 immunolabelling were not different in hypertrophy. Hypertrophied preparations showed local submillimeter (≈250 μm) regions with slow conduction and low intracellular conductance, which, although not affecting CV on the millimeter scale, were consistent with discontinuities from increased microscopical connective tissue content.

Conclusions—With myocardial hypertrophy, altered longitudinal and transverse CV, and greater nonuniformity of CV anisotropy correspond to changes of intracellular conductance. These are associated with alteration of myocardial architecture, specifically the topography of cell–cell coupling and gap-junction connectivity. **(*Circ Arrhythm Electrophysiol*. 2014;7:00-00.)**

Key Words: action potentials ■ connexin 43 ■ gap junctions ■ left ventricular hypertrophy ■ slowed nerve conduction velocity AQ6

In intact myocardium the 3-dimensional (3D) distribution of gap-junctions is a function of cellular architecture and distribution of cell–cell interactions, so that the topography of intracellular conductance is a major determinant of action potential (AP) propagation. Computational,[1] cell-culture,[2] and transgenic models[3] support this concept. The relationship between longitudinal and transverse conduction (conduction anisotropy) and small-scale nonuniformities are critical determinants of the arrhythmogenic substrate in ventricular and atrial myocardium.[4,5] Although not yet measured, the relationship between intracellular conductance, AP conduction, and myocardial architecture, and how they change in myocardial pathologies, is considered to be important to characterize the myocardial substrate for complex arrhythmias and the mechanistic understanding of fibrillation in particular. Such an integrated approach requires an appropriate model when changes to myocardial structure and AP conduction occur. Myocardial hypertrophy represents such a pathology, whereby alterations to connexin expression, cell and tissue architecture and AP propagation have been separately reported in different experimental models using various techniques to measure conduction.[6–12] However, these studies are often difficult to compare because of experimental differences. One study, using a model of nonischemic heart failure, did relate conduction velocity (CV) changes to myocyte dimensions and predict electrocardiographic changes.[13] We used a well-characterized model of myocardial hypertrophy to address the hypothesis that conduction anisotropy and nonuniformity is determined by changes of intracellular conductance, in turn determined by the cellular topography and distribution of gap junctions on the submillimeter and millimeter scale.

Clinical Perspective on p XXX

Received January 18, 2014; accepted September 9, 2014.

From the School of Physiology, Pharmacology, and Neuroscience, University of Bristol, Bristol, United Kingdom (C.H.F.); Department of Cardiovascular Medicine, Whittington Hospital, London, United Kingdom (R.P.G.); Department of Cardiology, Ashford and St Peter's NHS Foundation Trust, Chertsey, United Kingdom (P.S.D.); Department of Biochemistry and Physiology, University of Surrey, Surrey, United Kingdom (R.I.J.); and Myocardial Function Section, Imperial College London, London, United Kingdom (E.D., P.M.P., N.S.P.). AQ4

The Data Supplement is available at http://circep.ahajournals.org/lookup/suppl/doi:10.1161/CIRCEP.114.001471/-/DC1.

Correspondence to Christopher H. Fry, DSc, School of Physiology, Pharmacology, and Neuroscience, University of Bristol, University Walk, Bristol BS8 1TD, United Kingdom. E-mail chris.fry@bristol.ac.uk

Circ Arrhythm Electrophysiol **is available at http://circep.ahajournals.org** **DOI: 10.1161/CIRCEP.114.001471**

Methods

Methods are described in the Data Supplement.

Model of Ventricular Hypertrophy

Ventricular hypertrophy was induced in male Dunkin–Hartley guinea pigs (4 to 6 months), by placing a constricting clip around the ascending aorta. Sham controls underwent identical operations, but without clip placement.[14] Left ventricular papillary muscles were excised for electrophysiological recordings, and adjacent muscles placed in Zamboni fixative for morphological examination. These preparations were used because of their longitudinal fiber arrangement and less interstitial tissue. The investigation and surgical procedures conformed to the Guide for the Care and Use of Laboratory Animals (UK Animals Act, 1986, and the US National Institutes of Health; NIH publication No. 85-23, revised 1996), the study was approved by the Local Ethical Review Committee.

1D Intracellular Conductance and CV

Left ventricular preparations (0.5- to 0.9-mm diameter) were superfused (4 mL/min) with Tyrode solution at 36°C. Longitudinal CV, CV_L, was measured by stimulating the preparation at 1 end and recording multiple intracellular conducted AP at distances, d, >1 mm from the stimulating electrode. Conduction delay was the time, t, between stimulus artifact and dV/dt_{max} of the AP upstroke. CV_L was calculated from the slope of linear d versus t plots. Specific intracellular conductance was calculated from $G_i=(2CV_L\times 2C_m\times\tau_{ap})/a$[15], where a=myocyte radius, C_m=specific membrane capacitance, and τ_{ap}=time constant of the conducting AP subthreshold phase. Transverse CV, CV_T, was measured by stimulating with large Ag/AgCl electrodes on either side of the preparation; intracellular recordings were made perpendicular to the longitudinal axis[15] (Figure I in the Data Supplement).

3D Electrophysiological Measurements

Supra-threshold or subthreshold pulses were passed between 2 intracellular microelectrodes to measure CV or intracellular conductance (g), respectively. Interelectrode tip distance was measured within 20 μm (Figure II in the Data Supplement). The current-passing electrode remained in 1 cell and the recording electrode moved to 40 to 60 different sites to obtain 3D conduction or conductance maps. Impalement depth was measured to determine accurately interelectrode distance and incorporated into a 2D data display: the x axis corresponded to the longitudinal fiber axis and the y' axis to the distance $\sqrt{(y^2+z^2)}$, that is, y (transverse) and z (depth) axes were assumed equivalent.

Data are displayed in x- and y' planes as conduction delay isochrones or lines of equal conductance. The direction with the fastest CV and largest conductance per unit distance was the x axis. Perpendicular values were measured to estimate anisotropic ratios of conduction and conductance. In regions where conductance was relatively homogeneous the time course of membrane potential responses to subthreshold stimuli were fitted to a 3D solution of the cable equation (Figure 2A, see Results section).[16]

Western Blotting

Proteins from whole-tissue homogenates were resolved by 12% polyacrylamide sodium dodecyl sulfate polyacrylamide gel electrophoresis and transferred to polyvinylidene fluoride membranes. Membranes were incubated with connexin 43 (Cx43) primary antibody (polyclonal antimouse, Millipore; 1:1000 dilution) and subsequently with horseradish peroxidase–conjugated secondary antibody (goat antimouse, Millipore; 1:10 000 dilution). Protein bands were quantified by densitometric analysis, and normalized to corresponding actin protein densities, which were unaltered between control and left ventricular hypertrophy (LVH) animals.[17,18]

Connexin Immunohistochemistry

Preparations in Zamboni fixative were wax embedded. Hematoxylin and eosin–stained sections identified: tissue orientation, quantified tissue morphology, and cell dimensions. Myocyte cross-sectional areas were measured in ≥10 cells per section, from ≥5 sections per specimen.[19] Sections (10 μm) were labeled with a rabbit polyclonal E12H anti-Cx43 antibody,[20,21] (dilution 1:50). Cx40 and Cx45 immunolabelling used antibodies,[21,22] diluted 1:10 for Cx40 and 1:20 for Cx45. Secondary incubation was with antirabbit Cy3 (Chemicon International Inc, 1:500). TRITC-conjugated wheat-germ agglutinin (Sigma, 1:100) labeled cell membranes. Nuclei were labeled with the fluorescent nucleic acid–binding dye TO-PRO-3 (Invitrogen, 1:250).

Myocyte and Tissue Topology

A previously published method was used.[23] Preparations were fixed in Na cacodylate buffer (0.08 mmol/L), glutaraldehyde (2%), and $CaCl_2$ (2 mmol/L); postfixed in 1% osmium tetroxide; dehydrated and embedded in araldite resin. A series of 100 1-μm serial sections were cut in the plane longitudinal to the fiber axis, mounted sequentially and stained with methylene blue. For each sample, 6 separate index myocyte profiles were randomly selected in the 50th section and followed through the entire section series to identify the number of cells with which each index cell was coupled. Connective tissue percentage was estimated from sections fixed with 4% paraformaldehyde, stained with picrosirius red; relative areas of connective tissue and muscle were measured.

Quantification of Cx43 Signal Area

Confocal images of 6, randomly selected high-power (×630) fields of transversely sectioned tissue and an optical projection image of each en-face disk were examined to derive Cx43 signal area per disk and unit disk area. Cx43 signal density was total Cx signal area divided by total area occupied by myocytes. The Cx43 area per cell was calculated as total Cx43 signal area divided by cell dimensions.

Statistical Analyses

Values are medians (25, 75% interquartiles) with assumption about the normality of the data sets, n=number of hearts. Differences between sets were tested with Wilcoxon rank-sum tests, the null hypothesis was rejected at $P<0.05$. Specific P values are quoted except when $P<0.0001$. The association between 2 variables was assessed from the Spearman rank correlation coefficient, r.

Results

Heart-to-body weight ratio was greater in the aortic constriction (LVH) compared with the sham (control) group (4.8 [4.3, 5.3] versus 3.8 [3.5, 3.9] g/kg; n=13, 13; $P<0.0001$). There were no signs of LV failure (lung-to-body weight ratio 4.9 [4.2, 5.0] versus 4.6 [4.3, 4.8] g/kg; $P=0.28$) and no liver ascites. The greater heart-to-body weight ratio was mirrored by a larger cell diameter but no change to cell length (Table 1). T1

Quantitative Western blotting showed that overall Cx43 expression was similar in myocardium from control and LVH hearts (Figure 1A). The topography and 3D distribution of gap junctions was measured to correlate with changes to possible electrophysiological properties in hypertrophied myocardium. F1

Myocardial Topography and Distribution of Intercalated Disks

The general topographical arrangement of cells was preserved in hypertrophy; myocytes retained approximately cylindrical shapes, with a major intercalated disk at each end, but more lateral connections in LVH tissue (Figure 1B). Overall packing geometry and connectivity between adjacent cells were estimated from the number of adjacent cells with which an individual cell made intercalated disk contact. This was

Priyamalini	11/15/14	4 Color Fig(s): F1-2,5	13:37	Art:HAE001471

Table 1. Cell Dimensions, Distribution, and Morphology of Intercalated Disks and Cx43 Distribution in Control (n=12) and LVH (n=8) Myocardium: n=11 for Control Myocyte Diameter and Length AQ7

	Control	LVH	*P* Value
Cell diameter, μm	17.5 (15.7, 18.1)	21.1 (19.4, 21.8)	0.00019*
Cell length, μm	154 (116, 178)	147 (134, 166)	0.971
Cell contacts per cell	5.5 (5.4, 6.1)	8.6 (7.0, 9.1)	0.0039*
Intercalated disks per cell	8.3 (8.1, 8.6)	10.1 (9.1, 11.4)	0.00028*
Intercalated disk area, μm^2	30.9 (21.8, 38.5)	32.1 (21.6, 38.3)	1.000
Cx43 area per unit area of disk	0.30 (0.25, 0.32)	0.30 (0.22, 0.41)	0.972
Cx43 labeling, % WGA perimeter	2.6 (2.2, 3.3)	2.8 (2.7, 3.1)	0.851
Cx43 labeled area cell, μm^2	199 (189, 212)	252 (236, 335)	0.00031*
Lateral Cx43 labeling, % total	5.0 (4.2, 5.6)	24.0 (18.5, 26.2)	0.00025*

Median values (25, 75% interquartiles). Cx43 indicates connexin 43; and LVH, left ventricular hypertrophy. AQ8

*P<0.05 (LVH vs control).

significantly greater in hypertrophied samples, compared with control. Figure 1C shows a representative photomicrograph of the middle of 3 serial sections, with cell outlines drawn in adjacent panels, to illustrate the number and pattern of cell contacts with which a particular index cell (cell A in this example) makes contact. Cell A had 2 end-to-end abutments (cells D and G in the middle section); the number of end-to-end abutments per cell was unchanged in hypertrophy. The greater number of cells to which an individual myocyte makes contact in LVH myocardium was mirrored by more intercalated disks per cell (Table 1) from more lateral abutments. The greater number of cell-to-cell contacts in LVH tissue was not because of cell elongation (Table 1). However, the number of intercalated disks coupling any 2 adjacent cells was fewer in hypertrophy (1.48 [1.37, 15.5] versus 1.26 [1.07, 1.39]; P<0.0135) because of the greater number of separate cell contacts. Overall, with LVH tissue, a particular cell made side-to-side contact with more cells, but via fewer intercalated disks between any 2 cells.

Connexin Quantification and Distribution

The number of intercalated disks per cell was greater in LVH myocytes (Table 1). However, individual intercalated disks showed no significant architectural changes: disk area was similar, as was the proportion of intercalated disk labeled for Cx43. In addition, Cx43 labeling as a percentage of cell perimeter, the latter measured with wheat-germ agglutinin, was not different in LVH. However, the total area labeled for Cx43 was greater (Table 1) and reflects the larger membrane area of LVH myocytes and more intercalated disks. However, the amount of lateral Cx43 labeling was ≈5-fold more because of the greater number of lateral intercalated disks. Thus, myocyte hypertrophy was accompanied by more intercalated disks and Cx43 per myocyte. There was no significant difference to Cx43 density, commensurate with the above Cx43 expression data, but the greater absolute amount of Cx43 per cell was confined largely to lateral myocyte boundaries.

Cx40 immunolabelling was not detected in control or LVH hearts, but as a positive control was demonstrated in atrial tissue. Cx45 immunolabelling was indistinguishably sparse in control and hypertrophy myocardium.

1D CV and estimated intracellular conductance, G_i AQ9 Longitudinal CV, CV_L, was lower in LVH (60.5 [56.8, 70.1] versus 77.2 [75.8, 79.8] cm/s; n=12, 13; P=0.00242). This was also

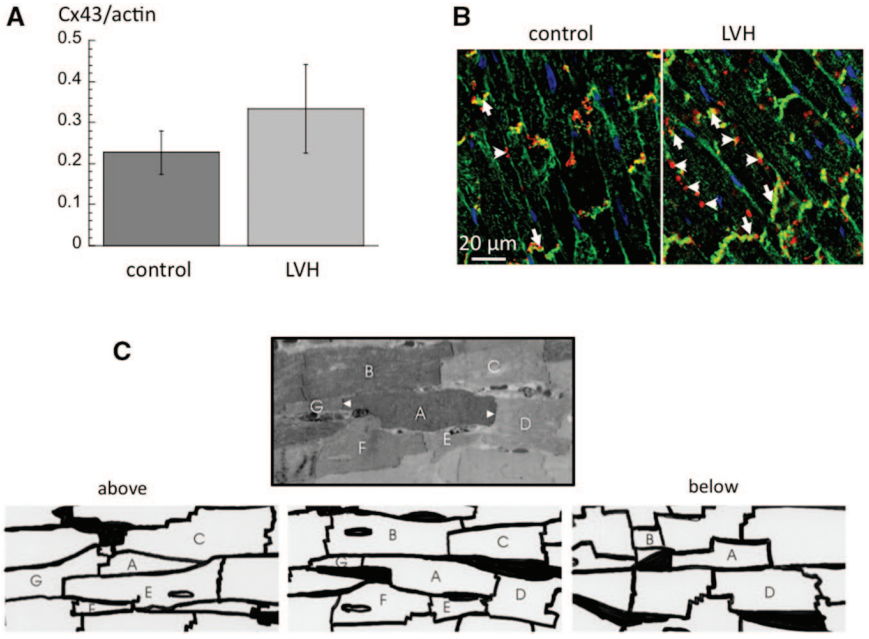

Figure 1. Connexin 43 (Cx43) and myocardial architecture. **A**, Cx43 protein expression, normalized to actin, for control and left ventricular hypertrophy (LVH) myocardium (n=8, 5; P=0.378). **B**, Confocal sections (left, control; right, LVH) immunolabelled for Cx43 (red), mainly confined to intercalated disks at ends of cells (arrows), or at lateral sites (arrowheads) especially in LVH. Cell membrane, green; nuclei, blue; cell membrane/Cx43 overlaps, yellow. **C**, Photomicrograph (×400) of an LVH myocardium section; shown is 1 from the middle of a consecutive series of one hundred 1-μm thick sections. Cell-to-cell interactions between an index cell (A) and its neighbors (B–G) traced through the whole cell thickness. Arrowheads mark intercalated disks and ends of cell A. Cartoons of this section and those immediately above and below are shown. AQ14

Priyamalini | 11/15/14 | 4 Color Fig(s): F1-2,5 | 13:37 | Art:HAE001471

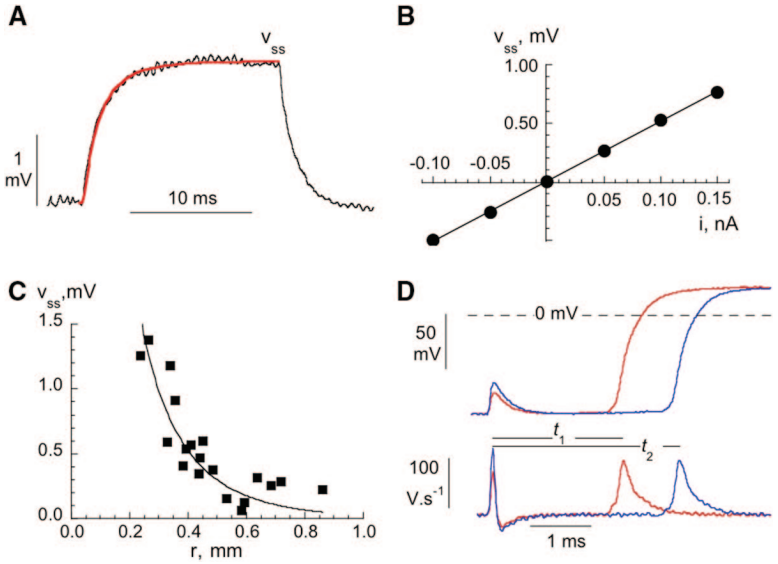

Figure 2. Intracellular stimulation and recording. **A**, subthreshold response to a 0.1 nA current; v_{ss}, steady-state response: line is a fit to the 3D cable equation $V(r,t)=\frac{k}{r}\left[e^{-r}\mathrm{erfc}\left(\frac{r}{2\sqrt{t}}-\sqrt{t}\right)+e^{r}\mathrm{erfc}\left(\frac{r}{2\sqrt{t}}+\sqrt{t}\right)\right]$; *r*, interelectrode distance; *k*, constant; erfc, complementary error function. **B**, current–voltage relationship of v_{ss} as a function of subthreshold current. **A** and **B**, *r*=200 μm. **C**, plot of v_{ss} (0.1 nA stimulation) as a function of interelectrode distance, *r*. Line is a plot of $v_{ss}=\frac{K}{r}\exp\frac{-r}{\lambda}$, λ=3D space constant, *K*=constant. **D**, upstroke phases of 2 action potentials and their first derivative with suprathreshold stimulation: t_1 and t_2 are delays for conduction to the 2 recording sites from the stimulus site, S. Distance between 2 recording electrodes 480 μm.

evident when both CV_L and transverse CV, CV_T, were measured together; CV_L was less (61.1 [57.9, 65.2] versus 76.6 [75.7, 79.3] cm/s; n=7, 8; *P*=0.00062) and CV_T greater (24.5 [21.7, 27.9] versus 18.7 [17.5, 19.8] cm/s; *P*=0.0114) in LVH. This resulted in a smaller conduction anisotropy ratio in LVH (CV_L/CV_T; 2.36 [2.22, 2.91] versus 4.20 [3.71, 4.61]; *P*=0.00075).

τ_{ap} was significantly smaller in transverse compared with longitudinal conducted APs, but in either axis were similar in LVH and control preparations (longitudinal, 0.27 [0.25, 0.28] versus 0.26 [0.26, 0.28] ms; *P*=0.820; transverse, 0.23 [0.22, 0.25] versus 0.24 [0.22, 0.26] ms; *P*=1.00). This excludes changes of ionic currents flowing during the AP upstroke as a cause of altered CV in LVH. Total intracellular specific conductivity, G_i, was estimated from longitudinally conducted APs and the 1D solution of the cable equation (see Methods section). G_i was significantly smaller in LVH (1.04 [0.64, 1.47] versus 2.17 [2.02, 2.47] mS/cm; *P*=0.00029) using values of *a*, τ_{ap}, and CV_L.

3D CV, CV_{3D}, and Intracellular Conductance, g_{3D}

F2 Figure 2 shows intracellular recordings from a preparation with uniform conduction and conductance characteristics, to test if data could be analyzed assuming a homogeneous spatial structure. A subthreshold stimulus response conformed to the transient solution of the 3D-cable equation (part A).[16] The relationship between steady-state response, v_{ss}, and stimulating current magnitude (*i*) was linear for subthreshold responses (part B). Values of v_{ss}, as a function of interelectrode distance, were fitted to a 3D solution of the cable equation (part C) and in 4 experiments yielded values for the 3D space constant of 0.31, 0.21, 0.19, and 0.16 mm. Part D shows the upstroke phase of APs from 2 intracellular recording sites a known distance (*d*) apart, and their differentials (d*V*/d*t*). CV was calculated from the ratio of *d* and difference in delays (t_2–t_1).

F3 Figure 3 shows anisotropy of conduction (part A) and intracellular conductance (part B) in control myocardium, with a primary (horizontal) axis of higher CV and conductance, and

T2 a perpendicular axis of minima. Table 2 shows CVs with an anisotropy ratio in control tissue (3.48 [3.11, 5.23]) similar to that measured with 1D conduction (3.84 [3.60, 4.07]), where the latter values were recorded on a supramillimetre scale. The 3D conductance ratio from subthreshold pulses was (3.95 [3.03, 5.29]). In LVH, CV in the primary axis was significantly smaller, but greater in the transverse axis (Table 2), corresponding with findings with 1D propagation. Intracellular conductance anisotropy was similarly smaller in LVH tissue.

Figure 4 shows the relationship between paired CV and con- F4
ductance anisotropy ratios for control (open circles) and LVH AQ10
(closed squares) data. For the control and LVH data combined, there was a significant association between these anisotropy ratios (*r*=0.95; n=15; *P*<0.0001). These data are therefore consistent with the hypothesis that variation in CV anisotropy depends on changes to anisotropy of intracellular conductance, with LVH values at the smaller region of the spectrum of values.

Figure 5 shows a phenomenon in several LVH preparations, F5
namely small-scale conduction (part A) and conductance (part B) discontinuities—where isochronal and isoconductance lines are bunched, indicating local regions of low intracellular conductance. This was not observed in sham-operated preparations, but was in

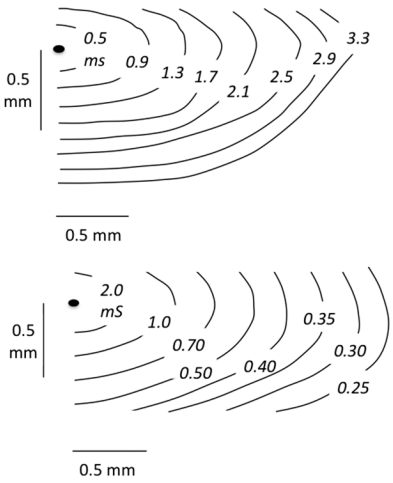

Figure 3. Conduction and conductance maps, normal myocardium (**A**) isochrones of conduction delays (ms). The black circle marks the stimulation point. **B**, lines of equal conductance (mS) for the same preparation.

Priyamalini	11/15/14	4 Color Fig(s): F1-2,5	13:37	Art:HAE001471

Table 2. Maximum and Minimum 3D CV or Conductance, *g*, and Anisotropy Values in Control (n=8) and LVH Myocardium (n=7)

	Control	LVH	*P* Value
CV_{max}, cm/s	54.5 (48.4, 64.7)	30.5 (27.6, 37.0)	0.00062*
CV_{min}, cm/s	11.2 (10.4, 11.9)	16.6 (14.7, 19.6)	0.0208*
CV anisotropy ratio	4.93 (4.37, 5.57)	1.81 (1.58, 2.52)	0.00015*
g_{max}, mS/cm	6.27 (4.80, 6.62)	3.50 (3.41, 4.76)	0.00257*
g_{min}, mS/cm	1.20 (0.99, 1.58)	1.70 (1.33, 1.96)	0.0247*
g anisotropy ratio	3.95 (3.03, 5.29)	1.87 (1.55, 2.42)	0.00062*

Median values (25, 75% interquartiles). CV indicates conduction velocity; and LVH, left ventricular hypertrophy.

*$P<0.05$ (LVH vs control).

5 of 12 LVH preparations. The submillimetre scale of the discontinuity would not affect macroscopic CV. Data from these high resistance regions were not included in Table 2, but they would accentuate conduction slowing and nonuniformity, and contribute further to a smaller intracellular conductance in the primary axis of LVH preparations. There was also more connective tissue in LVH preparations (11.7 [9.1, 16.0] versus 3.5 [3.2, 3.7]%; P=0.00025; AQ11 n=8, 12), appearing sometimes as longitudinally orientated septae between myocyte bundles (arrow, Figure 5C).

Relationships Between CV and Cx43 Expression

F6 Figure 6 shows paired data of 1D CV and Cx43 labeled area per myocyte. For control hearts data, none of the longitudinal and transverse CV, or the CV anisotropic ratio was associated with Cx43 area. For data from LVH hearts, longitudinal CV also was not significantly associated with Cx43 area. However, transverse CV was positively associated with Cx43 area, and the corresponding anisotropic ratio negatively associated with Cx43 area.

Discussion

The principal finding with this well-characterized model of myocardial hypertrophy was that both CV and intracellular conductance anisotropy were reduced and associated with changes to myocyte architecture, that is, more side-to-side Cx43 intercalated disks between larger myocytes, but each cell making contact with more neighboring cells.

Previous studies quantifying Cx43 in hypertrophic myocardium are conflicting, with increased, unchanged or reduced immunolabelled Cx43 per cell in different models, including human myocardium secondary to aortic stenosis.[10,17,24–26] These disparities probably result from differences in the duration and stimulus of hypertrophy, as well as species variability, and emphasize the need to study the relationship between AP conduction, intracellular conductance, and myocardial architecture in a single model and at greater resolution, as here.

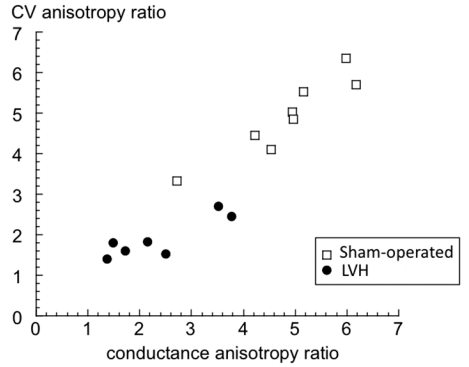

Figure 4. The relationship between conduction velocity (CV) and intracellular conductance anisotropy ratios. Data from control (open squares) and left ventricular hypertrophy (LVH; closed circles) myocardium, each point is a separate preparation.

There was a close correspondence between AP CV and intracellular conductance in both normal and hypertrophied myocardium. Previous studies using separate preparations to measure these variables only inferred this relationship,[8,9] but experiments directly demonstrated this and provides an electric basis for myocardial conduction anisotropy.

An additional notable finding was the change to the topography of cell contacts and gap junctions in hypertrophied myocardium. Although the number of intercalated disks per cell increased, the proportionately greater number of cell-to-cell contacts resulted in fewer intercalated disks between any 2 myocytes. The larger number of disks per cell has also been measured in human myocardium with concentric hypertrophy.[27] Ventricular myocardial cells are approximately cylindrical, with large intercalated disks at each end and smaller lateral disks. The basic cardiomyocyte shape, a cylinder with intercalated disks at both ends, is preserved in hypertrophy: thus, more intercalated disks per cell represents a greater number along the sides of the cell. The greater side-to-side connectivity and cell diameter are both consistent with the reduction in anisotropy of both conduction and intracellular conductance, as hypothesized by others.[28] This structural remodelling has also been observed in human hypertrophied myocardium,[17,21] and suggests that the observed electrophysiological changes may also occur in human tissue. Increased myocyte diameter in LVH (≈20%, Table 1) per se would enhance transverse CV at most by ≈9%. The actual increase of transverse CV by 48% (Table 2, CV_{min}) must therefore result mainly from gap-junction remodeling.

Although enhanced transverse coupling reduces charge available for longitudinal propagation, the architectural findings will not entirely explain the reduced longitudinal CV and associated reduction of intracellular conductance. With LVH intracellular longitudinal conductance, g_{max}, was reduced to ≈55%. Assuming cytoplasm and gap-junction conductance are in the ratio 3:1, and cytoplasm conductance is unaltered,[9,29] this represents more than a halving of unit gap junction conductance. There was no evidence of altered gap-junction structure, with respect to Cx43 immunolabelling, and so a reduced unit gap-junction conductance is proposed, including contributions from lowered intracellular pH[30,31] and dephosphorylation of gap-junction proteins.[32]

Reduced gap-junction conductance, and hence longitudinal current flow and AP propagation, could also contribute to enhanced transverse CV, by raising local intracellular current density. With a nonischemic model of heart failure longitudinal and transverse conduction velocities, as well as myocyte diameter, were increased,[13] suggesting that morphological changes alone could support these conduction changes, in contrast to data from this study that also requires changes to the electrophysiological properties of gap junctions.

There was also close concordance between directly measured intracellular conductance changes in hypertrophy and calculations using cable theory. Furthermore, cable theory accurately described

Priyamalini	11/15/14	4 Color Fig(s): F1-2,5	13:37	Art:HAE001471

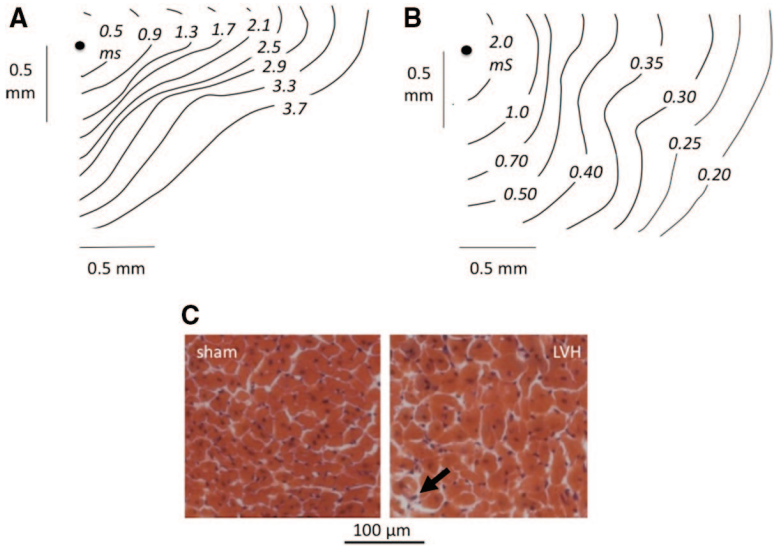

Figure 5. Conduction and conductance maps, left ventricular hypertrophy (LVH) myocardium (**A**) isochrones of conduction delays (ms). The black circle marks the stimulation point. **B**, lines of equal conductance (ms) for the same preparation. **C**: Sections of control and LVH myocardium; a small region of extracellular matrix in the LVH section is arrowed.

the time- and distance-dependent spread of subthreshold currents in a 3D continuum. However, in several hypertrophied preparations small-scale conduction and conductance discontinuities (<1 mm) were measured (Figure 6), which would not alter net CV, or be observable using extracellular recording techniques. However, the magnitude and abruptness of these changes will create nonuniformities of conduction that are recognized as important components of the arrhythmogenic myocardial substrate.[33]

Limitations

Papillary muscles were used because their arrangement of parallel myocardial fibres facilitated comparative electrophysiological and morphological measurements. However, extrapolation to other regions of the ventricle should be done. Moreover, the presence of Cx43 immunolabel at the cell membrane does not confirm localization at intercalated discs nor functional gap junctions.

Conclusions

AP CV in normal and hypertrophied myocardium is determined primarily by the conductance of the intracellular pathway. Changes to CV and intracellular conductance anisotropy in hypertrophy may be explained by altered myocyte and intercalated disk topography.

Acknowledgments

We acknowledge The British Heart Foundation ElectroCardioMaths Programme at Imperial College and the National Institute for Health Research Biomedical Research Centre Programme. AQ12

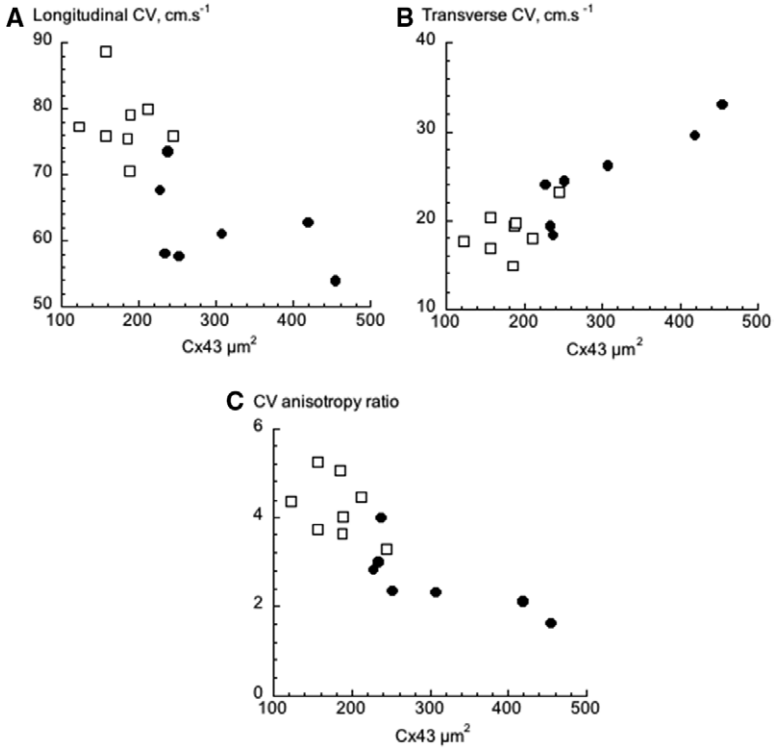

Figure 6. Association between connexin 43 (Cx43) area per cell and conduction velocity (CV). Control data open squares; left ventricular hypertrophy (LVH) data closed circles. **A**, longitudinal CV: control r=–0.071 (P>0.05); LVH r=–0.50 (P>0.05). **B**, transverse CV: control r=0.429 (P>0.05); LVH r=0.875 (P=0.01). **C**, anisotropic CV ratio: control r=–0.357 (P>0.05); LVH r=–0.875 (P=0.01).

Priyamalini	11/15/14	4 Color Fig(s): F1-2,5	13:37	Art:HAE001471

Sources of Funding

Thus study was funded by British Heart Foundation grants PG/08/065, RG/10/11/28457, and PG/12/64/29828.

Disclosures

None.

AQ13

References

1. Jongsma HJ, Wilders R. Gap junctions in cardiovascular disease. *Circ Res*. 2000;86:1193–1197.
2. Rohr S, Kucera JP, Kléber AG. Slow conduction in cardiac tissue, I: effects of a reduction of excitability versus a reduction of electrical coupling on microconduction. *Circ Res*. 1998;83:781–794.
3. Lo CW. Role of gap junctions in cardiac conduction and development: insights from the connexin knockout mice. *Circ Res*. 2000;87:346–348.
4. Peters NS, Wit AL. Myocardial architecture and ventricular arrhythmogenesis. *Circulation*. 1998;97:1746–1754.
5. Dillon SM, Allessie MA, Ursell PC, Wit AL. Influences of anisotropic tissue structure on reentrant circuits in the epicardial border zone of subacute canine infarcts. *Circ Res*. 1988;63:182–206.
6. Tamarappoo BK, John BT, Reinier K, Teodorescu C, Uy-Evanado A, Gunson K, Jui J, Chugh SS. Vulnerable myocardial interstitium in patients with isolated left ventricular hypertrophy and sudden cardiac death: a postmortem histological evaluation. *J Am Heart Assoc*. 2012;1:e001511.
7. Severs NJ, Dupont E, Thomas N, Kaba R, Rothery S, Jain R, Sharpey K, Fry CH. Alterations in cardiac connexin expression in cardiomyopathies. *Adv Cardiol*. 2006;42:228–242.
8. Botchway AN, Turner MA, Sheridan DJ, Flores NA, Fry CH. Electrophysiological effects accompanying regression of left ventricular hypertrophy. *Cardiovasc Res*. 2003;60:510–517.
9. Cooklin M, Wallis WR, Sheridan DJ, Fry CH. Changes in cell-to-cell electrical coupling associated with left ventricular hypertrophy. *Circ Res*. 1997;80:765–771.
10. Peters NS, Green CR, Poole-Wilson PA, Severs NJ. Reduced content of connexin43 gap junctions in ventricular myocardium from hypertrophied and ischemic human hearts. *Circulation*. 1993;88:864–875.
11. Spach MS, Heidlage JF, Barr RC, Dolber PC. Cell size and communication: role in structural and electrical development and remodeling of the heart. *Heart Rhythm*. 2004;1:500–515.
12. Formigli L, Ibba-Manneschi L, Perna AM, Pacini A, Polidori L, Nediani C, Modesti PA, Nosi D, Tani A, Celli A, Neri-Serneri GG, Quercioli F, Zecchi-Orlandini S. Altered Cx43 expression during myocardial adaptation to acute and chronic volume overloading. *Histol Histopathol*. 2003;18:359–369.
13. Wiegerinck RF, Verkerk AO, Belterman CN, van Veen TA, Baartscheer A, Opthof T, Wilders R, de Bakker JM, Coronel R. Larger cell size in rabbits with heart failure increases myocardial conduction velocity and QRS duration. *Circulation*. 2006;113:806–813.
14. Winterton SJ, Turner MA, O'Gorman DJ, Flores NA, Sheridan DJ. Hypertrophy causes delayed conduction in human and guinea pig myocardium: accentuation during ischaemic perfusion. *Cardiovasc Res*. 1994;28:47–54.
15. Carey PA, Turner M, Fry CH, Sheridan DJ. Reduced anisotropy of action potential conduction in left ventricular hypertrophy. *J Cardiovasc Electrophysiol*. 2001;12:830–835.
16. Jack JJB, Noble D, Tsien RW. *Electric Current Flow in Excitable Cells*. Oxford: Oxford University Press; 1975:218–223.
17. Kostin S, Dammer S, Hein S, Klovekorn WP, Bauer EP, Schaper J. Connexin 43 expression and distribution in compensated and decompensated cardiac hypertrophy in patients with aortic stenosis. *Cardiovasc Res*. 2004;62:426–436.
18. Dupont E, Matsushita T, Kaba RA, Vozzi C, Coppen SR, Khan N, Kaprielian R, Yacoub MH, Severs NJ. Altered connexin expression in human congestive heart failure. *J Mol Cell Cardiol*. 2001;33:359–371.
19. Baandrup U, Olsen EG. Critical analysis of endomyocardial biopsies from patients suspected of having cardiomyopathy. I: morphological and morphometric aspects. *Br Heart J*. 1981;45:475–486.
20. Harfst E, Severs NJ, Green CR. Cardiac myocyte gap junctions: evidence for a major connexon protein with an apparent relative molecular mass of 70,000. *J Cell Sci*. 1990;96(pt 4):591–604.
21. Severs NJ, Rothery S, Dupont E, Coppen SR, Yeh HI, Ko YS, Matsushita T, Kaba R, Halliday D. Immunocytochemical analysis of connexin expression in the healthy and diseased cardiovascular system. *Microsc Res Tech*. 2001;52:301–322.
22. Gros D, Jarry-Guichard T, Ten Velde I, de Maziere A, van Kempen MJ, Davoust J, Briand JP, Moorman AF, Jongsma HJ. Restricted distribution of connexin40, a gap junctional protein, in mammalian heart. *Circ Res*. 1994;74:839–851.
23. Luke RA, Saffitz JE. Remodeling of ventricular conduction pathways in healed canine infarct border zones. *J Clin Invest*. 1991;87:1594–1602.
24. Qu J, Volpicelli FM, Garcia LI, Sandeep N, Zhang J, Márquez-Rosado L, Lampe PD, Fishman GI. Gap junction remodeling and spironolactone-dependent reverse remodeling in the hypertrophied heart. *Circ Res*. 2009;104:365–371.
25. Kostin S, Rieger M, Dammer S, Hein S, Richter M, Klövekorn WP, Bauer EP, Schaper J. Gap junction remodeling and altered connexin43 expression in the failing human heart. *Mol Cell Biochem*. 2003;242:135–144.
26. Uzzaman M, Honjo H, Takagishi Y, Emdad L, Magee AI, Severs NJ, Kodama I. Remodeling of gap junctional coupling in hypertrophied right ventricles of rats with monocrotaline-induced pulmonary hypertension. *Circ Res*. 2000;86:871–878.
27. Yamamoto S, James TN, Sawada K, Okabe M, Kawamura K. Generation of new intercellular junctions between cardiocytes. A possible mechanism compensating for mechanical overload in the hypertrophied human adult myocardium. *Circ Res*. 1996;78:362–370.
28. Seidel T, Salameh A, Dhein S. A simulation study of cellular hypertrophy and connexin lateralization in cardiac tissue. *Biophys J*. 2010;99:2821–2830.
29. Dhillon PS, Gray R, Kojodjojo P, Jabr R, Chowdhury R, Fry CH, Peters NS. Relationship between gap-junctional conductance and conduction velocity in mammalian myocardium. *Circ Arrhythm Electrophysiol*. 2013;6:1208–1214.
30. Firek L, Weingart R. Modification of gap junction conductance by divalent cations and protons in neonatal rat heart cells. *J Mol Cell Cardiol*. 1995;27:1633–1643.
31. Wallis WR, Wu C, Sheridan DJ, Fry CH. Intracellular pH and H+ buffering capacity in guinea-pigs with left ventricular hypertrophy induced by constriction of the thoracic aorta. *Exp Physiol*. 1997;82:227–230.
32. Lim HW, De Windt LJ, Steinberg L, Taigen T, Witt SA, Kimball TR, Molkentin JD. Calcineurin expression, activation, and function in cardiac pressure-overload hypertrophy. *Circulation*. 2000;101:2431–2437.
33. Wit AL, Peters NS. The role of gap junctions in the arrhythmias of ischemia and infarction. *Heart Rhythm*. 2012;9:308–311.

CLINICAL PERSPECTIVE

Left ventricular hypertrophy (LVH) is associated with an increased risk of arrhythmias but the electrophysiological substrate in myocardium that underlies this significant clinical condition remains unclear. We have addressed the question using a well-validated guinea-pig model of LVH, after partial occlusion of the thoracic aorta. Action potential conduction anisotropy is a phenomenon whereby conduction is more rapid in a primary axis compared with perpendicular axes and in normal myocardium is a significant factor that minimizes arrhythmic re-entrant circuits. The data with LVH myocardium show that conduction anisotropy—measured with intracellular stimulating and recording electrodes—is reduced, slowed in the primary axis and unchanged or even increased in orthogonal axes. This electric remodeling occurs on a submillimeter scale and so would be less evident using extracellular recording methods. The loss of conduction anisotropy was mirrored by similar changes to the electric conductance of the intracellular space, the latter determined mainly by gap-junction electric properties. We attributed these electric changes in LVH myocardium to structural remodeling of the myocardium, with more transverse intercalated disks, along with reduced electric conductance of individual gap junctions. These data provide evidence that changes to the distribution and electric properties of gap junctions in LVH are a major contributor to changes of the electrophysiological substrate of myocardium that makes it prone to the development of arrhythmias.

AUTHOR QUERIES

AUTHOR PLEASE ANSWER ALL QUERIES

AQ1—Please note only those terms that are used 5 times or more can be abbreviated, except trial names, which should be expanded at first use but then can be abbreviated throughout regardless of how many times they appear.

AQ2—Please turn to page 3 of your proof and review the running head, which will appear in the upper right-hand margins of odd-numbered pages. Running heads must be 50 or fewer characters in length, including spaces and punctuation. If your original short title was longer than 50 characters, we may have shortened it. Please modify if necessary (but observe our length guidelines).

AQ3—Please confirm that all authors are included in the correct order in the byline and that all names are spelled correctly, including special characters, accents, middle initials, and degrees, if applicable. Note that journal style discourages listing American honorary degrees in the byline; such degrees are deleted during editing.

AQ4—Please confirm that all authors' institutional affiliations (including city/state/country locations) are correct as shown in the affiliations footnote.

AQ5—Per style, italics should not be used for emphasis. Hence, it has been removed where used. Please confirm if the change made is correct.

AQ6—Key words have been edited to match the US National Library of Medicine's Medical Subject Headings (http://www.nlm.nih.gov/mesh/MBrowser.html). If they need modification, please refer to this site and limit the total number of key words to 7.

AQ7—Please review the typeset tables carefully against copies of the originals to verify accuracy of editing and typesetting.

AQ8—Per style, italics should not be used for emphasis. Hence, it has been removed in Tables 1 and 2 and represented as footnotes *. Please confirm if the change made is correct.

AQ9—Per style, bold should not be used for emphasis. Hence, it has been removed where used. Please confirm if the change made is correct.

AQ10—Note that in the artwork of Fig 4, closed circles and open squares were only provided. But in the text, they were explained as open circles and closed squares. Please check.

AQ11—Per style, quotes should not be used for emphasis. Hence, they have been deleted in the article. Please confirm whether the change made is appropriate.

AQ12—Please carefully review any Acknowledgments, Sources of Funding, and/or Disclosures listed at the end of the manuscript (before the References), and confirm that they are accurate and complete for all authors.

AQ13—Refs 13 ans 33 seem to be identical. Hence, we have deleted Ref. 33 and renumbered the references both in text and list. Please check.

AQ14—We've identified that all figures are low resolution and could result in poor-quality graphics in the final publication. Please send higher-resolution versions of these figures, or approve to proceed with the figure(s) as shown in your proof.